



Photocurrent generation based on new tetrathiafulvalene–BODIPY dyads

Keijiro Tsujimoto, Reiko Ogasawara, Hideki Fujiwara*

Department of Chemistry, Graduate School of Science, Osaka Prefecture University, Gakuen-cho, Naka-ku, Sakai 599-8531, Japan

ARTICLE INFO

Article history:

Received 16 November 2012
Revised 14 December 2012
Accepted 20 December 2012
Available online 3 January 2013

Keywords:

Organic conductors
Photofunctional materials
Optical properties
Photo-electric conversion
Photoconductors

ABSTRACT

New donor–acceptor dyads containing tetrathiafulvalene (TTF) and 4,4-difluoro-4-bora-3a,4a-diaza-s-indacene (BODIPY) moieties were synthesized to develop new photoconducting materials. More than half of fluorescence from the BODIPY part was quenched by the photo-induced intramolecular electron transfer from the TTF part to the BODIPY part. Photoelectrochemical measurements indicate that cathodic photocurrents can be generated from a thin film of the dyad spin-coated on ITO electrode. Crystal structure analysis of the ethylenedithio–TTF derivative indicated two-dimensional conducting pathways are constructed in the TTF-stacking layer, and photocurrent measurement indicated that photo-induced conductivity enhancement can be achieved in this crystal.

© 2012 Elsevier Ltd. All rights reserved.

In this decade, the development of tetrathiafulvalene (TTF)-acceptor dyads has drawn much interest in the fields of optoelectronic materials because the combination of the electron-donating (D) TTF frameworks and several kinds of functional electron-accepting (A) parts such as fluorophores, C₆₀, polar compounds, and chelating ligands, has expanded the possibility of novel functional materials such as chemical/physical sensors, molecular rectification, fluorescence switches, photovoltaic cells, and nonlinear optical devices.^{1–5} For the application to the photofunctional devices such as photovoltaic cells, the photoinduced intramolecular electron transfer (PET) process between the TTF and acceptor parts has been recognized as the crucial key step for the indispensable formation of charge separated state.^{6,7} Among them, we have studied the development of photofunctional organic materials exhibiting photo-induced conductivities and photo-electric conversion functionalities using the TTF-based D–A type hybrid molecules for the future use of photo-sensors and photovoltaic applications. Recently, we have synthesized new TTF derivatives substituted with 2,5-diphenyl-1,3,4-oxadiazole (PPD),^{8,9} 1,3-benzothiazole (BTA),¹⁰ and fluorene moieties,¹¹ which show a strong fluorescence in the UV region and can be used as an antenna for photoexcitation. We found that these D–A type hybrid molecules can exhibit photo-induced conductivities and photo-electric conversions through the photo-induced charge-transfer.¹² On the other hand, we focused on the 4,4-difluoro-4-bora-3a,4a-diaza-s-indacene (BODIPY) moiety and its derivatives¹³ that are known to show quite a strong absorption in the visible region, high photo- and chemostability and have

been used for fluorescent switches/probes and dye-sensitized solar cells.^{14–17} Therefore, we designed new π -conjugated D–A type dyads containing TTF and BODIPY moieties (Chart 1: **1a**, **b**) to realize novel photofunctional materials. In this Letter, we report the synthesis, photo-electric conversional properties, structure, and photo-induced conductivities of dyads **1a**, **b**. Furthermore, we also report on the crystal structure analysis and photoinduced conductivity using a single crystal of compound **1b**.

BODIPY-substituted TTF derivatives **1a**, **b** were synthesized as described in Scheme 1. TTF and ethylenedithio–TTF (EDT–TTF) were converted into the corresponding tributylstannyl derivatives (**2a**, **b**) by the reported conventional method.^{18,8} Then, the Stille coupling reaction between the tributylstannyl derivatives (**2a**, **b**) and *p*-bromophenyl-BODIPY (**3**)¹⁹ was performed under toluene reflux using Pd(PPh₂)Cl₂ as a catalyst to obtain BODIPY–phenyl-substituted derivatives **1a**, **1b** in 52% and 22% yields, respectively, after the separation by the silica gel column-chromatography.

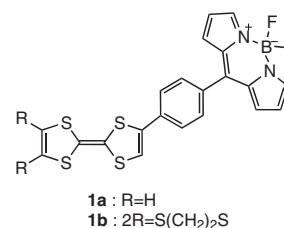
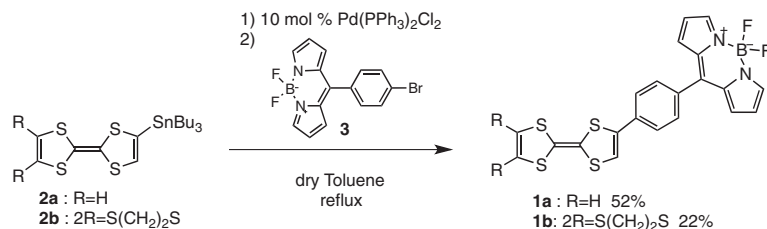


Chart 1. Molecular structure of **1a**, **b**.

* Corresponding author. Tel./fax: +81 72 254 9818.

E-mail address: [hfuj@c.s.osakafu-u.ac.jp](mailto:hfuji@c.s.osakafu-u.ac.jp) (H. Fujiwara).

Scheme 1. Synthesis of compounds **1a**, **b**.

The electrochemical properties of **1a**, **b** were investigated by the cyclic voltammetry technique in benzonitrile at 25 °C. The dyads showed three pairs of one-electron reversible redox waves (E_{red} , E_{ox1} and E_{ox2}) and one irreversible wave (E_{ox3}) as summarized in Table 1. The redox potentials E_{ox1} and E_{ox2} of **1a** are almost the same to those of TTF (+0.41 and +0.80 V) under the identical condition, and the redox potentials E_{red} and E_{ox3} are also the same as those of BODIPY derivative **3** (−0.70 and +1.67 V), suggesting that the first and second oxidations (ox1 and ox2) occur at the TTF part and the third one (ox3) occurs at the BODIPY part. These results suggest that the HOMO orbital of dyads **1a**, **b** mainly locates on the TTF part and these donors have a good enough electron-donating ability.

UV–vis absorption spectra of the 10^{−5} M CHCl₃ solution of dyads **1a**, **b** were measured at room temperature as shown in Figure 1. Dyads **1a**, **b** showed a very strong absorption maximum at 505 nm with ϵ values more than 40,000 mol^{−1} L cm^{−1} that corresponds to the π – π^* transition of the BODIPY part, because the same absorption maximum was usually observed around 505 nm in many BODIPY derivatives^{13,20} like *p*-bromophenyl-substituted BODIPY **3**. On the other hand, a broad absorption shoulder was observed above 550 nm in dyads **1a**, **b**. Because this shoulder absorption was not observed in TTF and BODIPY derivatives **3**, this absorption can be assigned to the intramolecular charge-transfer (ICT) transition between the HOMO that localizes on the TTF part to the LUMO that localizes on the phenyl–BODIPY part. Due to this broad absorption manner through all the visible region, dyads **1a**, **b** show a dark black color in its solid and solution state.

Emission spectra of **1a**, **b**, BODIPY derivative **3** were measured in 10^{−6} M CHCl₃ solutions at room temperature. Wavenumbers of maximum absorption peaks (λ_{max}), emission peaks (λ_{em}), and 0–0 transition energy (E_{0-0}) were summarized in Table 2. When the solution of BODIPY derivative **3** was irradiated by the excitation light of 505 nm that corresponds to the absorption maximum of BODIPY, quite a strong fluorescence was observed around 516 nm. However, in the case of the CHCl₃ solution of **1a**, **b**, more than a half of their fluorescence intensities that originate from the BODIPY moiety was quenched as shown in Figure 2. This result suggests that the fluorescence from the excited BODIPY (BODIPY*) part is diminished by the intramolecular electron transfer process from the electron-donating TTF part to the BODIPY* part because

Table 1
Redox potentials (V) of **1**, TTF, and **3**^a

Compound	E_{red}	E_{ox1}	E_{ox2}	E_{ox3}	$E_{\text{ox2}}-E_{\text{ox1}}$
1a	−0.69	+0.43	+0.82	+1.65 ^b	0.39
1b	−0.68	+0.51	+0.85	+1.67 ^b	0.34
TTF		+0.41	+0.80		0.39
3	−0.70			+1.67 ^b	

^a V versus Ag/AgCl, 0.1 mol L^{−1} *n*-Bu₄NClO₄ in benzonitrile at 25 °C, Pt electrodes, scan rate of 50 mV s^{−1}. The potentials were corrected with Ferrocene; $E(\text{Fc}/\text{Fc}^+) = +0.48$ V versus Ag/AgCl.

^b Irreversible step.

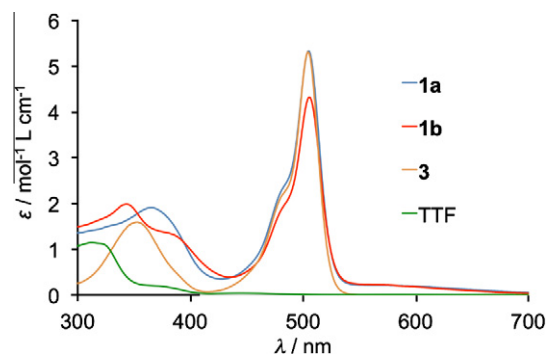
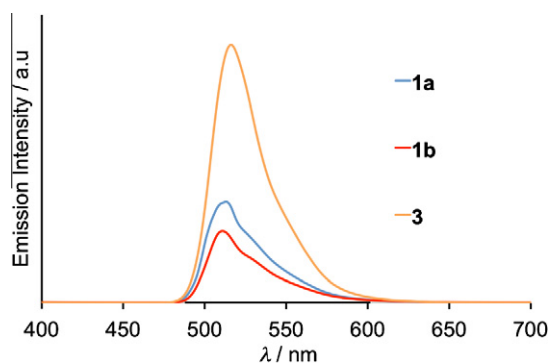
Figure 1. UV–vis absorption spectra of **1a**, **b**, **3** and TTF in 10^{−5} M CHCl₃ solution.

Table 2
Wavenumbers of maximum absorption peaks (λ_{max}), emission peaks (λ_{em}), and 0–0 transition energy (E_{0-0})^a

Molecule	λ_{max} (nm)	λ_{em} (nm)	E_{0-0} (eV)
1a	269, 367, 505	513	2.44
1b	343, 505	511	2.44
3	275, 353, 504	516	2.44

^a 0–0 transition energy (E_{0-0}) was estimated from the cross position of the absorption and emission spectra.

Figure 2. Emission spectra of **1a**, **b** and **3** in 10^{−6} M CHCl₃ solution.

the fluorophores such as BODIPY* part possess the electron-accepting ability upon excitation.^{21–23} Gibbs free energy for such a photo-induced electron transfer process (PET) ΔG_{PET} can be estimated to be a large negative value of ca. −1.4 eV using the Rehm–Weller equation,²⁴ $\Delta G_{\text{PET}} = e[E_{\text{ox1}} - E_{\text{red}}] - E_{0-0} - C$, where C is a Coulombic term (~ 0.1 eV). This estimation suggests that this PET process is thermodynamically favorable in the case of dyads **1a**, **b**. However, compared to the cases of the other TTF-fluorescent part dyads such as a TTF–PPD⁸ in which almost all the fluorescence of PPD part was quenched, the twisted molecular structure between the TTF part and phenyl–BODIPY part will weaken the intramolecular

interaction upon excitation as discussed later. The other TTF–BODIPY hybrid molecule was also recently reported by Lorcay and co-workers, in which the methyl-substituted BODIPY part is directly connected to the trimethyl–TTF without any spacer.²⁵ In this molecule, almost no ICT transition was observed above 550 nm and the emission from the BODIPY part was not quenched at all. These results are quite different from our results and will originate from a very weak intramolecular interaction caused by a largely twisted molecular structure between the TTF and BODIPY parts due to the steric hindrance between the methyl-substituted BODIPY part and the methyl group of the TTF part.

Molecular orbital calculation and the simulation of UV–vis spectra of dyad **1a** were performed on the basis of the DFT theory and the TD–DFT method (B3LYP/6-31+G*) using GAUSSIAN 09 package.²⁶ The molecular structure in chloroform was optimized using the SCRF method with the polarizable continuum solvation model (PCM). The optimized molecular structure has a twisted structure and the torsional angles between planes are large, 22° for TTF–phenyl, 55° for phenyl–BODIPY, and 38° for TTF–BODIPY. These angles, especially the angle for TTF–BODIPY planes, are similar to those obtained in the crystalline state of **1b** as mentioned later and suggested that the weakened π – π interaction between the TTF and BODIPY parts results in the imperfect quenching of fluorescence. The atomic coefficients of HOMO and LUMO orbitals of **1a** are almost localized on the TTF and BODIPY parts, respectively (see Supplementary data). The HOMO–LUMO gap energy is calculated to be 1.77 eV from the energy levels of HOMO (–5.01 eV) and LUMO (–3.24 eV). The TD–DFT calculation qualitatively reproduces the intramolecular charge-transfer (ICT) character of the lowest energy absorption around 600 nm, although the λ_{max} (ICT) value is strongly underestimated to be 848 nm. On the other hand, a very strong absorption at 505 nm is cleared to originate from the transitions from the BODIPY-based HOMO-1 (6.28 eV) to LUMO and from HOMO-2 (–6.50 eV) to LUMO orbitals.

To investigate the photo-electric conversion functionality of the synthesized molecules, measurements of photocurrents based on thin films of dyads **1a**, **b** were performed by a photoelectrochemical method. Thin films of dyads **1a**, **b** were spin-coated on a ITO-glass substrate and were used as a working electrode in 0.5 M aqueous KCl solution.²⁷ Platinum and Ag/AgCl electrodes were used as counter and reference electrodes, respectively. As shown in the photocurrent action spectra for the thin film of **1a** (Fig. 3), positive photocurrent maxima of 240 nA around 370 nm, 470 nA around 500 nm, and 40 nA around from 600 to 750 nm were observed under –0.30 V bias voltage versus Ag/AgCl. These maxima roughly correspond to the absorption maxima of the identical thin-films of **1a** on ITO electrode (see also Fig. 3), suggesting that the absorbed photons were converted into electric currents on the thin-films of the dyads on ITO electrode as a result of the

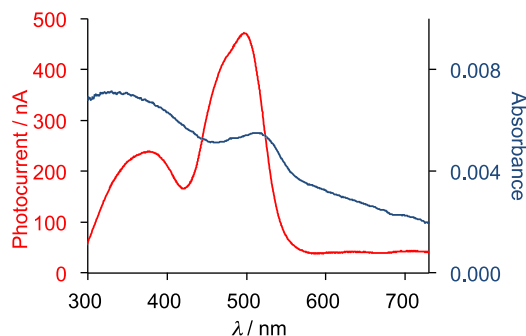


Figure 3. Photocurrent action spectrum under –0.30 V bias voltage versus Ag/AgCl reference electrode and absorption spectrum of the thin film of **1a** spin-coated on ITO electrode.

charge transfer process between the TTF and BODIPY parts. The observed positive photocurrents suggest that the electron transfers from the conduction band of the ITO electrode (–4.5 eV)²⁸ to the hole generated on the dyads upon photo-irradiation. The wavelength dependence of these photocurrents is quite similar to the UV–vis spectra of dyad **1a** which shows absorption maxima at the same wavelength around 370 and 500 nm, indicating that this photocurrent action spectrum reflects the optical properties of the independent molecule (not the condensed state). The photocurrent conversion efficiency from the absorbed photons to electric currents was calculated to be 1.7% at 505 nm for **1a** from the value of maximum photocurrent ($I_{\text{max}} = 469 \text{ nA/cm}^2$) and the absorbance of the thin film used ($Abs = 0.0054$) and the power of irradiated light (6.9 mW/cm^2),²⁹ whereas dyad **1b** showed a lower efficiency of 0.80% at 505 nm. Although these efficiencies are similar to that of TTF–PPD dyad (1.6% at 330 nm under bias voltage of –0.4 V versus Ag/AgCl),⁸ dyads **1a**, **b** showed photocurrent maxima in the middle of the visible region around 500 nm, indicated that dyads **1a**, **b** are much more effective for the conversion of visible region of sun light.

An X-ray crystal structure analysis of **1b** was performed using its dark green plate-like single crystal recrystallized from CS₂/*n*-pentane.³⁰ This crystal belongs to the monoclinic $P2_1/a$ space group, and there is one crystallographically independent molecule in the unit cell. Figure 4 shows the molecular structure of **1b**. The TTF part has a boat-form conformation with a bent angle of 19.2° and 16.1° at the sulfur positions, whereas the phenyl and BODIPY moieties have high planarity with maximum differences from their least square planes (0.015 and 0.054 Å, respectively). On the other hand, torsional angles between these parts are large, 45° for TTF–phenyl, 53° for phenyl–BODIPY, and 34° for TTF–BODIPY, suggesting that the π – π interaction between the TTF and BODIPY parts may be also weakened in the crystalline state of **1b**. As Figure 5 indicates, dyad **1b** forms a stacking structure in a head-to-tail manner along the *b*-axis and there are also side-by-side interactions between these stacking columns along the *a*-axis. Because there are several short S–S contacts between the sulfur atoms of the TTF moieties in the stacking direction and between the neighboring columns, there is a two-dimensional intermolecular interaction between the TTF parts in the *ab*-plane (see also Fig. 6).

Overlap integrals between the neighboring TTF parts were calculated on the basis of the extended Hückel approximation (see Fig. 6). The overlap integrals along the *b*-axis [$b_1 = 15.3$, $b_2 = 4.61$, $b_3 = 1.98 (\times 10^{-3})$] and along the *a*-axis ($a = 1.98 \times 10^{-3}$) indicate that uniform (b_3) and dimerized (b_1 and b_2) interactions between the TTF parts coexist along the stacking *b*-axis, and a uniform side-by-side interaction exists along the *a*-axis. Due to these relatively large intermolecular interactions between the TTF parts, this crystal is expected to show photo-induced conductivity along both the *a*- and *b*-axes upon photoirradiation.

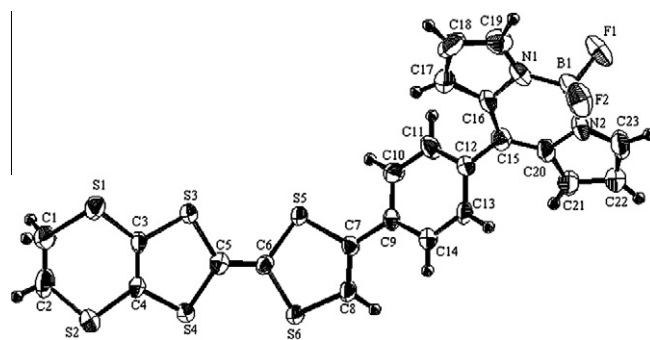


Figure 4. ORTEP drawing of the molecule in the crystal of **1b**.

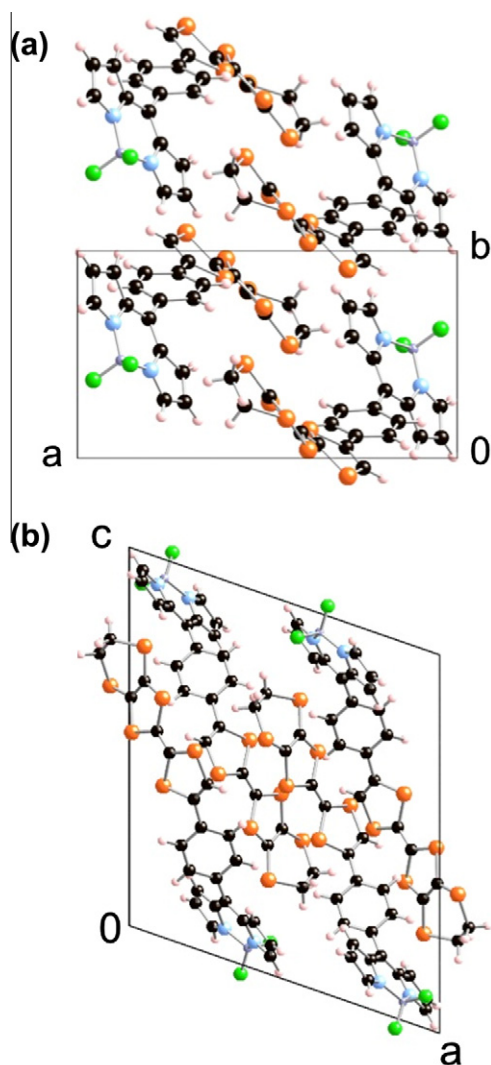


Figure 5. Packing structure of **1b** (a) view from *c*-axis (b) View from *b*-axis.

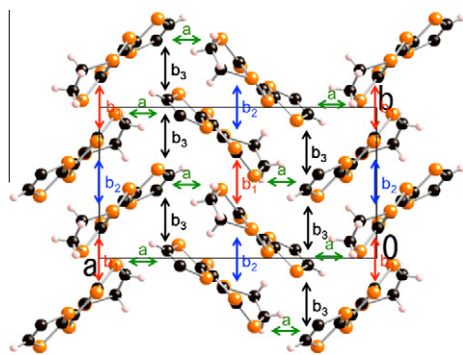


Figure 6. Overlap integrals between the TTF parts in **1b**.

To investigate the photoconductivity of the single crystal of **1b**, photocurrent measurements were performed by the two terminal method along the *b*-stacking columns and the side-by-side direction along the *a*-axis. Electrical contacts were achieved with two gold wires (length between the terminals: 33 μm) and increases of currents under a chopped white-light irradiation from 300 W Xe lamp (21.8 mW cm^{-2} , 300–600 nm) were measured under an application of 50 V between two terminals. As shown in Figure 7,

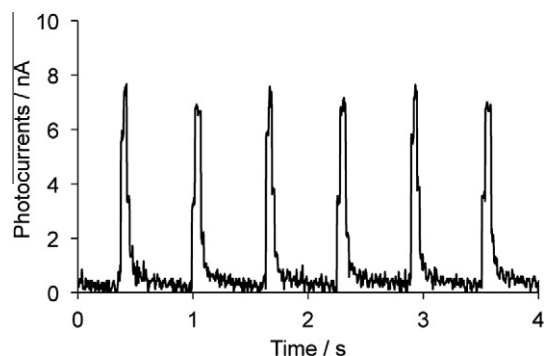


Figure 7. Photocurrent changes upon irradiation of the chopped white light (300–600 nm) to the single crystal of **1b** measured along the *b*-axis.

sharp changes of electrical currents upon irradiation, that is, photocurrent generations of ca. 7 nA along the *b*-axis were observed according to the irradiation of the chopped light (ca. 1.5 Hz). These sudden increases and decreases are considered to be driven by the transient carriers generated by the photo-induced charge transfers and the following slow decreases of currents are considered to originate from the cooling relaxation process of the thermal effect of the irradiation. The current increases of 7 and 11 nA measured along the *b*- and *a*- axes, respectively, resemble each other, suggesting that the uniform intermolecular interactions (b_3 and a) may mainly mediate the carrier transfers. These values correspond to the conductivity change of this crystal from $3.4 \times 10^{-7} \text{ S cm}^{-1}$ under dark to $3.9 \times 10^{-7} \text{ S cm}^{-1}$, and from $9.3 \times 10^{-7} \text{ S cm}^{-1}$ under dark to $10.2 \times 10^{-7} \text{ S cm}^{-1}$, along the *b*- and *a*-axes, respectively. These results indicated the conductivity increase of ca. 10–15% along these two directions and suggest the two-dimensional conducting nature in the *ab*-plane of this crystal. Even though the values of photocurrents are not so large, these results suggest that the single crystal of **1b** can cause photoconductivities along the *ab*-conduction plane of the layer structure of TTF parts by the photoinduced intramolecular electron transfer and the resultant charge-separated state.

In conclusion, we have synthesized new TTF-based D–A type dyads containing a highly fluorescent BODIPY part. The photoelectrochemical measurements on the spin-coated thin film of **1a** suggest that positive photocurrents can be generated by the PET process between the TTF and BODIPY parts. Furthermore, we also observed photocurrent generations along the *b*- and *a*-axes according to the irradiation of the chopped light on the single crystalline sample of **1b**, reflecting the two-dimensional conducting nature in the *ab*-plane of this crystal. These results suggest that the TTF-based D–A dyads can be regarded as good candidates for optoelectronic materials such as photo-electric conversion materials and photoconducting applications.

Acknowledgments

This work was financially supported in part by Grants-in-Aid for Scientific Research (Nos. 20110006 and 21750150) from the Ministry of Education, Culture, Sports, Science and Technology of Japan, and by Grant for Young Researcher from JGC-S Scholarship Foundation.

Supplementary data

Supplementary data (experimental section, molecular orbitals, crystallographic data) associated with this article can be found, in the online version, at <http://dx.doi.org/10.1016/j.tetlet.2012.12.097>. These data include MOL files and InChIKeys of the most important compounds described in this article.

References and notes

1. Brunetti, F. G.; Lopez, J. L.; Atienza, C.; Martin, N. *J. Mater. Chem.* **2012**, *22*, 4188–4205.
2. Gorgues, A.; Hudhomme, P.; Salle, M. *Chem. Rev.* **2004**, *104*, 5151–5184.
3. Segura, J. L.; Martin, N. *Angew. Chem., Int. Ed.* **2001**, *40*, 1372–1409.
4. Wenger, S.; Bouit, P.-A.; Chen, Q.; Teuscher, J. L.; Censo, D. D.; Humphry-Baker, R.; Moser, J.-E.; Delgado, J. L.; Martin, N.; Zakeeruddin, S. M.; Grätzel, M. *J. Am. Chem. Soc.* **2010**, *132*, 5164–5169.
5. Yamada, J.; Sugimoto, T. *TTF Chemistry: Fundamentals and Applications of Tetrathiafulvalene*; Kodansha-Springer: Tokyo, 2004.
6. Bryce, M. R. *Adv. Mater.* **1999**, *11*, 11–23.
7. Nishikawa, H.; Kojima, S.; Kodama, T.; Ikemoto, I.; Suzuki, S.; Kikuchi, K.; Fujitsuka, M.; Luo, H. X.; Araki, Y.; Ito, O. *J. Phys. Chem. A* **2004**, *108*, 1881–1890.
8. Fujiwara, H.; Sugishima, Y.; Tsujimoto, K. *Tetrahedron Lett.* **2008**, *49*, 7200–7203.
9. Fujiwara, H.; Sugishima, Y.; Tsujimoto, K. *J. Phys. Conf. Ser.* **2008**, *132*, 012025.
10. Fujiwara, H.; Yokota, S.; Hayashi, S.; Takemoto, S.; Matsuzaka, H. *Physica B* **2010**, *405*, S15–S18.
11. Fujiwara, H.; Tsujimoto, K.; Sugishima, Y.; Takemoto, S.; Matsuzaka, H. *Physica B* **2010**, *405*, S12–S14.
12. Furukawa, K.; Sugishima, Y.; Fujiwara, H.; Nakamura, T. *Chem. Lett.* **2011**, *40*, 292–294.
13. Loudet, A.; Burgess, K. *Chem. Rev.* **2007**, *107*, 4891–4932.
14. Golovkova, T. A.; Kozlov, D. V.; Neckers, D. C. *J. Org. Chem.* **2005**, *70*, 5545–5549.
15. Thivierge, C.; Han, J. Y.; Jenkins, R. M.; Burgess, K. *J. Org. Chem.* **2011**, *76*, 5219–5228.
16. Hattori, S.; Ohkubo, K.; Urano, Y.; Sunahara, H.; Nagano, T.; Wada, Y.; Tkachenko, N. V.; Lemmetyinen, H.; Fukuzumi, S. *J. Phys. Chem. B* **2005**, *109*, 15368–15375.
17. Erten-Ela, S.; Yilmaz, M. D.; Icli, B.; Dede, Y.; Icli, S.; Akkaya, E. U. *Org. Lett.* **2008**, *10*, 3299–3302.
18. Iyoda, M.; Kuwatani, Y.; Ueno, N.; Oda, M. *J. Chem. Soc., Chem. Commun.* **1992**, 158–159.
19. Pena-Cabrera, E.; Aguilar-Aguilar, A.; Gonzalez-Dominguez, M.; Lager, E.; Zamudio-Vazquez, R.; Godoy-Vargas, J.; Villanueva-Garcia, F. *Org. Lett.* **2007**, *9*, 3985–3988.
20. Karolin, J.; Johansson, L. B. A.; Strandberg, L.; Ny, T. *J. Am. Chem. Soc.* **1994**, *116*, 7801–7806.
21. Farren, C.; Christensen, C. A.; FitzGerald, S.; Bryce, M. R.; Beeby, A. *J. Org. Chem.* **2002**, *67*, 9130–9139.
22. Wang, C. S.; Bryce, M. R.; Batsanov, A. S.; Stanley, C. F.; Beeby, A.; Howard, J. A. K. *J. Chem. Soc., Perkin Trans. 2* **1997**, 1671–1678.
23. Loosli, C.; Jia, C. Y.; Liu, S. X.; Haas, M.; Dias, M.; Levillain, E.; Neels, A.; Labat, G.; Hauser, A.; Decurtins, S. *J. Org. Chem.* **2005**, *70*, 4988–4992.
24. Rehm, D.; Weller, A. *Isr. J. Chem.* **1970**, *8*, 259.
25. Huang, K. L.; Bellec, N.; Guerro, M.; Camerel, F.; Roisnel, T.; Lorcy, D. *Tetrahedron* **2011**, *67*, 8740–8746.
26. Frisch, M. J.; Trucks, G. W.; Schlegel, H. B.; Scuseria, G. E.; Robb, M. A.; Cheeseman, J. R.; Scalmani, G.; Barone, V.; Mennucci, B.; Petersson, G. A.; Nakatsuji, H.; Caricato, M.; Li, X.; Hratchian, H. P.; Izmaylov, A. F.; Bloino, J.; Zheng, G.; Sonnenberg, J. L.; Hada, M.; Ehara, M.; Toyota, K.; Fukuda, R.; Hasegawa, J.; Ishida, M.; Nakajima, T.; Honda, Y.; Kitao, O.; Nakai, H.; Vreven, T.; Montgomery, J. A., Jr.; Peralta, J. E.; Ogliaro, F.; Bearpark, M.; Heyd, J. J.; Brothers, E.; Kudin, K. N.; Staroverov, V. N.; Keith, T.; Kobayashi, R.; Normand, J.; Raghavachari, K.; Rendell, A.; Burant, J. C.; Iyengar, S. S.; Tomasi, J.; Cossi, M.; Rega, N.; Millam, J. M.; Klene, M.; Knox, J. E.; Cross, J. B.; Bakken, V.; Adamo, C.; Jaramillo, J.; Gomperts, R.; Stratmann, R. E.; Yazyev, O.; Austin, A. J.; Cammi, R.; Pomelli, C.; Ochterski, J. W.; Martin, R. L.; Morokuma, K.; Zakrzewski, V. G.; Voth, G. A.; Salvador, P.; Dannenberg, J. J.; Dapprich, S.; Daniels, A. D.; Farkas, O.; Foresman, J. B.; Ortiz, J. V.; Cioslowski, J.; Fox, D. J.; GAUSSIAN 09, Revision B.01, Gaussian, Inc., Wallingford, CT, 2010.
27. These films were prepared on an ITO-coated soda-lime glass substrate (surface resistance 70–100 Ω /sq) by a spin-coating method (spin-coated area: 1.0 \times 0.8 cm) using 1 mL of 1 g/L solution of the donors in CHCl_3 at 2000 rpm for 60 s.⁸ Photocurrents between the working and counter electrodes were measured by a BAS Electrochemical Analyzer Model 612B under irradiation from 150 W Xe lamp where monochromatized light in the wavelength range from 300 to 730 nm was produced by holographic monochromators using a fluorescence spectrometer JASCO FP-6200.
28. Thompson, W. G.; Anderson, R. L. *Solid State Electron.* **1978**, *21*, 603–608.
29. Li, F. Y.; Jin, L. P.; Huang, Y. Y.; Huang, C. H.; Zheng, J.; Guo, J. Q. *J. Mater. Chem.* **2001**, *11*, 1783–1788.
30. Crystal data for **1b**: chemical formula: $\text{C}_{23}\text{H}_{15}\text{BN}_2\text{F}_2\text{S}_6$, $F_w = 560.55$, monoclinic, $P2_1/a$, $a = 16.1840(13)$, $b = 8.3409(5)$, $c = 18.7005(13)$ Å, $\beta = 109.193(2)^\circ$, $V = 2384.1(3)$ Å³, $Z = 4$, $D_{\text{calcd}} = 1.562$ g/cm³, 5260 unique reflections the final R and R_w were 0.0663 and 0.0445 (3923 reflections [$I > 2.0\sigma(I)$]).